Ionic Liquids Hot Paper

International Edition: DOI: 10.1002/anie.201501715
German Edition: DOI: 10.1002/ange.201501715

Potential-Dependent Adlayer Structure and Dynamics at the Ionic Liquid/Au(111) Interface: A Molecular-Scale In Situ Video-STM Study**

*Rui Wen, Björn Rahn, and Olaf M. Magnussen**

Abstract: *Room-temperature ionic liquids are of great current interest for electrochemical applications in material and energy science. Essential for understanding the electrochemical reactivity of these systems are detailed data on the structure and dynamics of the interfaces between these compounds and metal electrodes, which distinctly differ from those in traditional electrolytes. In situ studies are presented of Au(111) electrodes in 1-butyl-1-methylpyrrolidinium bis(trifluoromethylsulfonyl)imide ([BMP][TFSA]) by high-speed scanning tunneling microscopy (video-STM). [BMP][TFSA] is one of the best-understood air and water stable ionic liquids. The measurements provide direct insights into the potential-dependent molecular arrangement and surface dynamics of adsorbed $[BMP]^+$ cations in the innermost layer on the negatively charged Au electrode surface. In particular, two distinct subsequent transitions in the adlayer structure and lateral mobility are observed with decreasing potential.*

Room-temperature ionic liquids (RTILs) offer a promising combination of properties, including low vapor pressure, wide electrochemical windows, and tunable polarity, which make them highly attractive compounds in the field of electrochemistry, for example, in electrodeposition, batteries, nanoscience, and solar cells.[1] In these applications, the molecular structure and dynamic behavior of the ionic liquid near the interface to the electrode have been shown to strongly influence electrochemical reactions, for example, electrochemical deposition processes, and thus play an essential role in determining the system performance.[2] For a deeper insight into the structure–reactivity correlation, detailed data on the molecular-scale interface structure and dynamics at metal/RTILs interfaces is necessary, which is a subject of substantial current research.[2d,3] Recent experimental[4] and theoretical studies[3c,5] revealed a multilayer architecture that exhibits fundamental differences compared to the electrochemical double layers found in aqueous and organic electrolytes.

Experimental data on the RTIL interfacial structure has been obtained by in situ scanning tunneling (STM) and atomic force (AFM) microscopy,[4a–d,f,6] ex situ STM under ultrahigh vacuum (UHV) conditions,[7] vibrational spectroscopy,[8] and X-ray and neutron reflectometry.[9] However, the molecular arrangement of the molecules on the electrode surface could only be clarified in a few cases.[6b,10] Even less is known on the structural dynamics within these adlayers. Electrochemical impedance spectroscopy measurements indicated parallel capacitive processes on different time scales,[2b,3d,e] but direct data on the molecular scale adlayer dynamics are still largely missing. The in situ video-STM technique developed by our group has in the past enabled detailed studies of the dynamic processes (up to the millisecond range) in ionic and molecular adlayers at metal electrodes in aqueous electrolyte solutions.[11] It is employed here for molecular resolution studies on the 100 ms time scale of the [BMP][TFSA]/Au(111) interface, a well-understood system with attractive properties for applications.[9c,12]

In agreement with previous electrochemical measurements,[2e] Au(111) in [BMP][TFSA] has a wide electrochemical window (Figure 1), extending over a potential region from −3.2 to 2.3 V vs. the Pt quasi-reference electrode (experimental procedures and additional electrochemical data are given in the Supporting Information). In potential sweeps in the negative direction starting at the open-circuit

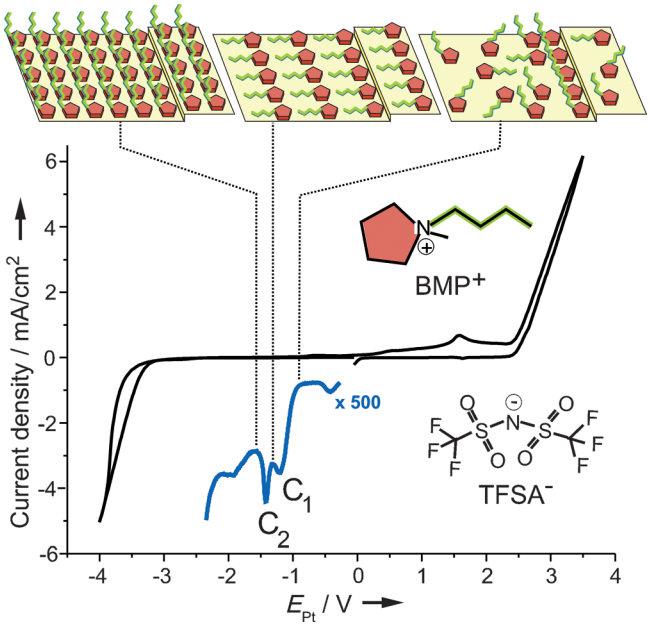

Figure 1. Cyclic voltammogram of Au(111) in [BMP][TFSA] recorded at a scan rate of 10 $mV s^{-1}$. The models above indicate the surface phase transitions associated with current peaks C_1 and C_2 (only the $[BMP]^+$ cations are shown for clarity).

[*] Dr. R. Wen, B. Rahn, Prof. Dr. O. M. Magnussen
Institute of Experimental and Applied Physics, Kiel University
Olshausenstrasse 40, 24098 Kiel (Germany)
E-mail: magnussen@physik.uni-kiel.de

[**] We thank the Deutsche Forschungsgesellschaft for financial support via MA1618/15. R.W. gratefully acknowledges a scholarship from Alexander von Humboldt Foundation.

Supporting information for this article is available on the WWW under http://dx.doi.org/10.1002/anie.201501715.

© 2015 Wiley-VCH Verlag GmbH & Co. KGaA, Weinheim

potential, two cathodic peaks (C_1 and C_2) are observed in the potential region between −0.35 V and −1.7 V, which were assigned in earlier studies of this[4b] and other $[BMP]^+$ containing RTILs[2b,3e,4a] to unknown surface processes occurring during $[BMP]^+$ adsorption. As we will show in the following, these cathodic peaks are associated with changes in the molecular arrangement of adsorbed $[BMP]^+$ in the innermost layer on the Au electrode surface (represented above the voltammogram in Figure 1).

High-resolution in situ video-STM studies enable direct observations of the molecular arrangement and dynamics at the [BMP][TFSA]/Au(111) interface, revealing a strong dependence on the potential (see the Supporting Information for details on the video-STM measurements, data analysis, and interpretation). Stable images could only be obtained at potentials ≤ -1.0 V. At −1.0 V, no molecular scale structures could be resolved on atomically smooth Au terraces. However, in the vicinity of Au steps, strongly fluctuating adlayer structures with a locally ordered arrangement could occasionally be observed (Figure 2). These ordered areas consist

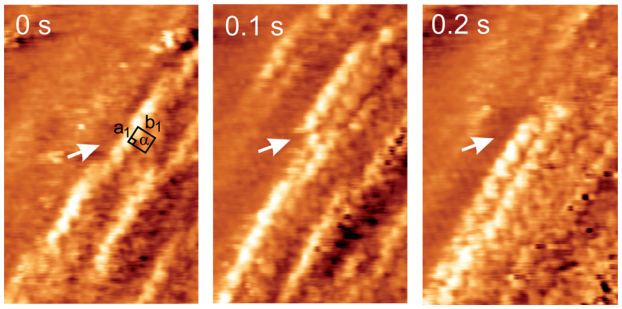

Figure 2. Subsequent images (3.8 nm × 6.1 nm) taken from an in situ video-STM on Au (111) in [BMP][TFSA] at −1.0 V.

of one to three molecular rows in which a rectangular adlayer structure with lattice spacings of $a_1 = 0.47 \pm 0.05$ and of $b_1 = 0.49 \pm 0.05$ nm is visible (Figure 2, 0.1 s). As will be justified in more detail below, we associate the individual maxima in this adlayer structure with the heterocylic ring of the $[BMP]^+$ cation. Because the size of the unit cell is too small for $[BMP]^+$ in a fully planar adsorption geometry, it is proposed that only the ring of the $[BMP]^+$ cations is directly adsorbed on the surface in this structure. The molecular rows along each step edge exhibit significant changes on the 100 ms time scale and usually could only be observed consecutively for subsecond periods in the video-STM experiments. We attribute these equilibrium fluctuations to attachment/detachment of molecules on the lower terrace to the step itself or to molecular rows already attached to steps, respectively.

Decreasing the potential to −1.4 V, that is, into the potential range between the cathodic peaks C_1 and C_2, results in distinct changes in the molecular adlayer. Now extended domains of a two-dimensional ordered structure are visible on atomically flat terraces of the Au substrate (Figure 3a). The unit cell distances are $a_2 = 0.51 \pm 0.05$ and $b_2 = 1.01 \pm 0.05$ nm, with an angle of $78 \pm 2°$ with respect to each other, which fits well to the molecular size of the $[BMP]^+$ cation and

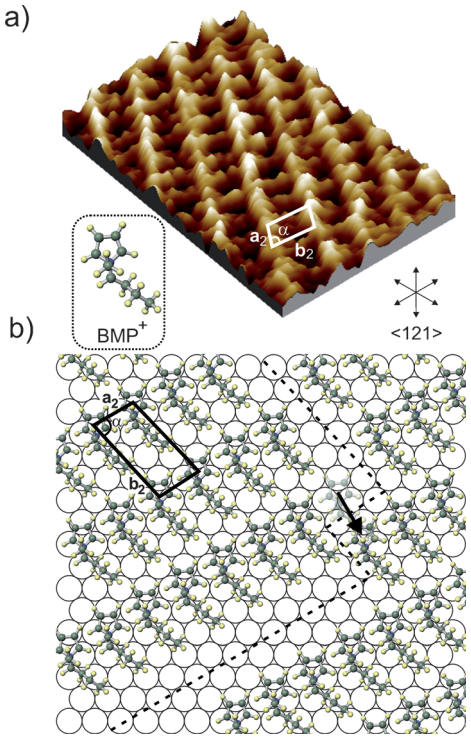

Figure 3. a) High-resolution STM image (5.4 nm × 7.5 nm) of the $[BMP]^+$ adlayer on Au(111) at −1.4 V and b) proposed structural model, showing two domains of the $(\sqrt{3} \times \sqrt{13})$ $[BMP]^+$ adlayer separated by a translational domain boundary (indicated by dashed line).

corresponds to 0.52 nm^2 per molecule or a coverage of 1.9 nm^{-2}, respectively. The more close-packed molecular rows along the "a_2 direction" are parallel to the ⟨121⟩ direction of the underlying Au (111) lattice. These structural parameters are in good agreement with a $(\sqrt{3} \times \sqrt{13})$ adlayer superstructure, formed by $[BMP]^+$ adsorption in a planar configuration (Figure 3b). The prominent maximum in each unit cell is assigned to the heterocylic ring of the $[BMP]^+$, the weaker chain-like structure along the "b_2 direction" to the alkyl chains. Similar prominent maxima were observed by Uhl et al. in a UHV-STM study of coadsorbed $[BMP]^+$ cations and $[TFSA]^-$ anions at 100 K and likewise attributed to the heterocylic ring of a $[BMP]^+$ cation in planar adsorption geometry.[7b,13] This molecular arrangement also is in agreement with previous force–distance measurements by AFM, where planar $[BMP]^+$ adsorption was inferred from the height of the innermost layer.[2b,4a,b]

Although the adlayer structure at −1.4 V is more stable than that found at −1.0 V, rapid dynamic fluctuations can be observed at defects and domain boundaries in the $(\sqrt{3} \times \sqrt{13})$ $[BMP]^+$ adlayer. This is illustrated by two sequences of images, selected from STM video sequences (available in the Supporting Information), which were obtained in areas with translational domain boundaries oriented predominantly along the b_2 direction (Figure 4a) and along the a_2 direction (Figure 4b), respectively. In both cases the domains are shifted along the a_2 direction by circa $b_2/2$ with respect to each other, whereas no significant shift between the $[BMP]^+$

 © 2015 Wiley-VCH Verlag GmbH & Co. KGaA, Weinheim

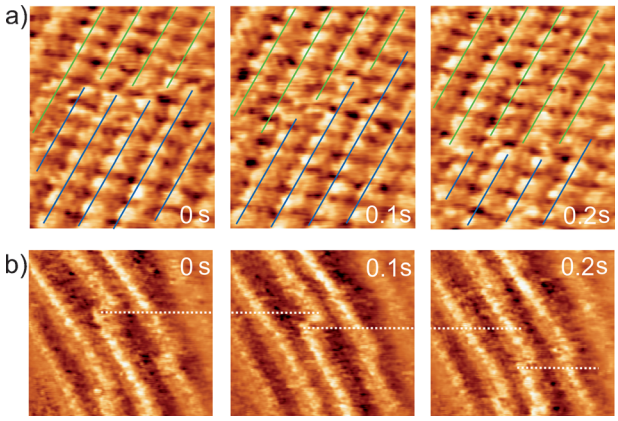

Figure 4. Subsequent images taken from in situ video-STM sequences at −1.4 V, recorded at domain boundaries along a) b_2 direction (4.5 nm × 6.6 nm) and b) a_2 direction (6 nm × 5.4 nm). Lines in (a) illustrate the lateral shift of the upper (green) to the lower (blue) domain; the dashed lines in (b) mark the motion of the center rows.

adsorbates of the two domains is found along the b_2 direction, suggesting a domain structure as indicated in the model in Figure 3b. Boundaries parallel to the close-packed molecular rows along a_2 are much straighter and considerably less mobile than those oriented along b_2. Temporal changes seem to occur exclusively at the terminations of the a_2 oriented rows, which change in length by several unit cell distances between subsequent images. These equilibrium dynamic processes at constant potential can be rationalized by the transfer of $[BMP]^+$ cations across the domain boundary by a translation on the surface along b_2 (as indicated by arrow in Figure 3b).

Upon a further negative shift in potential to −1.6 V, a transition to a different well-ordered molecular arrangement of $[BMP]^+$ on the Au (111) electrode is observed (Figure 5a). It can be described by a rectangular unit cell with

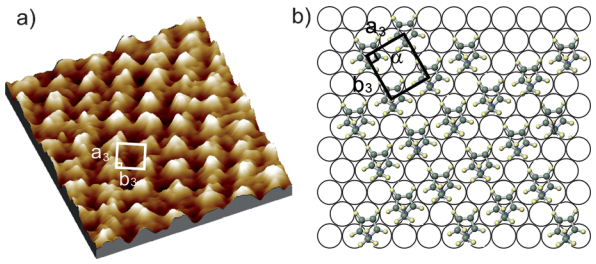

Figure 5. a) High-resolution STM image (4 nm × 4 nm) of the $[BMP]^+$ adlayer on Au(111) at −1.6 V and b) proposed structural model (only the heterocyclic ring of the $[BMP]^+$ cations is shown).

unit cell distances $a_3 = 0.50 \pm 0.05$ and $b_3 = 0.55 \pm 0.05$ nm, respectively. This corresponds to a space requirement of 0.275 nm^2 per molecule or a surface density of 3.6 nm^{-2}, that is, an increase in coverage by 90% with respect to the $(\sqrt{3} \times \sqrt{13})$ structure. The structural parameters of the adlayer at −1.6 V are in good agreement with a $(\sqrt{3} \times 2)$ superstructure (illustrated in Figure 5b). Because of the high packing density, a fully planar adsorption of $[BMP]^+$ in this structure is not possible. However, the unit cell size agrees well with the size of the heterocyclic ring. We therefore propose that at these negative potentials the positively charged ring is adsorbed on the Au surface, while the alkyl chains are oriented upright. Dynamic fluctuations of the type seen at −1.4 V could not be observed in the regime of the $(\sqrt{3} \times 2)$ adlayer, suggesting that the lateral mobility in this highly packed structure is further decreased.

Our video-STM observations are in good agreement with recent results from simulations and experimental studies by other techniques. According to these previous studies, on the neutral electrode both anions and cations are located in the innermost layer on the surface, but even in this potential range predominantly the organic cations are adsorbed.[4a,5b] We propose that this type of interface structure is present at potentials positive of the current peak C_1. The ordered molecular rows observed at −1.0 V near Au steps suggest a stronger adsoption of the $[BMP]^+$ cations at these surface defects. This may be caused by chemical as well as electrostatic interactions: The former would be expected owing to the more open atomic structure at the steps as compared to the close-packed Au (111) surface, the latter because of the electric dipole moment associated with steps on metal surfaces, which should lead to an increased attraction of the ions. Based on the orientation of this dipole moment, which results in an increased electron density at the bottom of the step, adsorption of the cations at the lower terrace side of the step should be favored, as indeed seems to be suggested by the STM observations. Interestingly, the interaction is sufficiently strong to temporarily stabilize up to three molecular rows near the step. The dense packing in these rows suggests an arrangement with the ring adsorbed on the Au, either in a planar or tilted geometry, and the hydrocarbon chains pointing away from the surface. The rapid attachment/detachment of molecules at these rows suggests that the surface mobility in the adlayer is high at this potential (in the inner parts of the Au terraces apparently too high for direct video-STM observations of the molecules).

The formation of an ordered $(\sqrt{3} \times \sqrt{13})$ $[BMP]^+$ adlayer in which the molecules adopt a fully planar adsorption geometry likewise is in accordance with current insight into the RTIL/electrode interface structure. Potential-induced transitions in the adlayer on the electrode surface have been also reported for other RTILs with similar cations. Surface-enhanced Raman scattering[8] and sum frequency generation[3a,14] studies in 1-*n*-butyl-3-methylimidazolium hexafluorophosphate ([BMI][PF_6]) found changes from an end-on to a surface-parallel orientation of the imidazolium ring with decreasing potential. This change to a planar cation adsorption at negative potentials can be explained by the improved charge screening, made possible by this geometry, that is, the minimization of the distance between the heterocylic ring on which the cation charge is located to the counter charge on the electrode surface. The transition to a second structure with an even higher $[BMP]^+$ surface density at potentials negative of peak C_2 can be likewise attributed to electrostatic effects, specifically an increase in the first layer charge density owing to the higher negative charge on the Au electrode. This behavior is in accordance with molecular

 © 2015 Wiley-VCH Verlag GmbH & Co. KGaA, Weinheim

dynamics simulations, which found that at low charge densities the ionic liquid cations in the first layer are oriented preferentially parallel to the interface, whereas at high negative electrode charges some of the cations tend to be oriented perpendicular to the surface as a consequence of the increased packing density of the ions.[5b]

The lateral structure of the $(\sqrt{3}\times\sqrt{13})$ adlayer indicates a stripe-like arrangement of the $[BMP]^+$ molecules, in which close-packed rows of the heterocyclic rings and rows of the attached alkyl chains alternate. A similar structure has been previously observed for [BMI], albeit with a double-row arrangement where the alkyl chains of two neighboring rows are facing each other.[10a] Such structures may be interpreted as a nanoscale separation into polar and nonpolar regions on the Au surface. In the bulk of RTILs such separation (albeit without long-range order) is well-established by experimental and simulation studies (see Ref. [15] for a detailed overview). On the metal surface, this separation may be assisted by epitaxial effects, for example, a preference of the molecules for specific adsorption sites of the Au(111) lattice. In the more closely packed $(\sqrt{3}\times 2)$ structure the surface is fully covered by the polar rings and the nonpolar chains have to be displaced into the layer above. Within this picture the $(\sqrt{3}\times\sqrt{13})\rightarrow(\sqrt{3}\times 2)$ transition would correspond to a transition from a lateral to a vertical nanoscale separation of polar and nonpolar regions. The density in a $(\sqrt{3}\times 2)$ layer of extended alkyl chains is sufficiently low to allow the additional presence of $[TFSA]^-$ anions in this second layer. The almost square structure of the $[BMP]^+$ cations on the hexagonal Au(111) substrate seems at a first glance surprising and would not be expected on the basis of packing arguments. However, as shown by previous studies in aqueous electrolytes,[16] a square adlayer arrangement provides optimal lateral screening for a mixed (bi)layer of monovalent cations and anions and therefore should be energetically preferred. Within the conceptual framework of modern theories of the RTIL/electrode,[5b] this lateral order may be interpreted as the consequence of overscreening, where the electrode charge is overcompensated by the innermost layer of the RTIL, resulting in a series of alternating layers of opposite charge near the interface.[17]

The rapid dynamic fluctuations observed by video-STM may be one of the reasons why molecular resolution images up to now have been rarely obtained in conventional in situ STM. At potentials more positive than −1.0 V, the surface mobility of the adsorbed $[BMP]^+$ cations seems to be too high to enable imaging even by video-STM, which agrees with the liquid-like behavior found by UHV-STM for [BMP][TFSA] on Au(111) at room temperature.[7b,13] The decrease in adlayer mobility towards more negative potentials most likely reflects the higher packing density and the increased attraction of the cations to the surface, which should result in lower exchange of these species with the RTIL bulk and higher activation barriers for surface diffusion. Even in the presence of dynamic fluctuations the molecules exhibit a strong preference for maintaining configurations, in which the ring and alkyl chain are aligned with those of neighboring $[BMP]^+$ (see Figure 3b, arrow). This again can be rationalized by the tendency for separation into nanoscale polar and nonpolar regions on the surface, which seems to be an important structural motive for the adayer at these intermediate surface charges.

In conclusion, our video-STM results support current models of the RTIL/metal interface structure and provide detailed insight into the potential-dependent structure as well as dynamic behavior. The lateral arrangement of the molecules in the ionic liquid near the electrode surface seems to be determined by the subtle interplay of charge screening, polar–nonpolar segregation, and epitaxial effects, resulting in distinct structural transitions at potentials of peaks C_1 and C_2 in the voltammogram. Such changes in interface structure and dynamics may be expected also in related RTIL systems. Precise microscopic data on these phenomena, as determined here for $[BMP]^+$, will be essential for understanding the electrochemical reactivity at the RTIL/electrode interface on the molecular scale.

Keywords: electrochemistry · gold · in situ video STM · ionic liquids · surface dynamics

How to cite: *Angew. Chem. Int. Ed.* **2015**, *54*, 6062–6066
Angew. Chem. **2015**, *127*, 6160–6164

[1] a) D. R. Macfarlane, M. Forsyth, P. C. Howlett, J. M. Pringle, J. Sun, G. Annat, W. Neil, E. I. Izgorodina, *Acc. Chem. Res.* **2007**, *40*, 1165–1173; b) M. Armand, F. Endres, D. R. MacFarlane, H. Ohno, B. Scrosati, *Nat. Mater.* **2009**, *8*, 621–629; c) P. Wang, S. M. Zakeeruddin, I. Exnar, M. Gratzel, *Chem. Commun.* **2002**, 2972–2973; d) F. Endres, S. Z. El Abedin, *Phys. Chem. Chem. Phys.* **2006**, *8*, 2101–2116; e) S. F. L. Mertens, C. Vollmer, A. Held, M. H. Aguirre, M. Walter, C. Janiak, T. Wandlowski, *Angew. Chem. Int. Ed.* **2011**, *50*, 9735–9738; *Angew. Chem.* **2011**, *123*, 9909–9912.

[2] a) M. Mezger, H. Schroder, H. Reichert, S. Schramm, J. S. Okasinski, S. Schoder, V. Honkimaki, M. Deutsch, B. M. Ocko, J. Ralston, M. Rohwerder, M. Stratmann, H. Dosch, *Science* **2008**, *322*, 424–428; b) R. Atkin, N. Borisenko, M. Drueschler, F. Endres, R. Hayes, B. Huber, B. Roling, *J. Mol. Liq.* **2014**, *192*, 44–54; c) Y.-Z. Su, Y.-C. Fu, Y.-M. Wei, J.-W. Yan, B.-W. Mao, *ChemPhysChem* **2010**, *11*, 2764–2778; d) M. V. Fedorov, A. A. Kornyshev, *Chem. Rev.* **2014**, *114*, 2978–3036; e) F. Endres, O. Hoefft, N. Borisenko, L. H. Gasparotto, A. Prowald, R. Al-Salman, T. Carstens, R. Atkin, A. Bund, S. Z. El Abedin, *Phys. Chem. Chem. Phys.* **2010**, *12*, 1724–1732.

[3] a) S. Baldelli, *Acc. Chem. Res.* **2008**, *41*, 421–431; b) F. Endres, N. Borisenko, S. Z. El Abedin, R. Hayes, R. Atkin, *Faraday Discuss.* **2012**, *154*, 221–233; c) V. Ivaništšev, M. V. Fedorov, R. M. Lynden-Bell, *J. Phys. Chem. C* **2014**, *118*, 5841–5847; d) B. Roling, M. Drueschler, B. Huber, *Faraday Discuss.* **2012**, *154*, 303–311; e) M. Drüschler, N. Borisenko, J. Wallauer, C. Winter, B. Huber, F. Endres, B. Roling, *Phys. Chem. Chem. Phys.* **2012**, *14*, 5090–5099.

[4] a) R. Atkin, N. Borisenko, M. Drueschler, S. Z. El Abedin, F. Endres, R. Hayes, B. Huber, B. Roling, *Phys. Chem. Chem. Phys.* **2011**, *13*, 6849–6857; b) R. Atkin, S. Z. El Abedin, R. Hayes, L. H. S. Gasparotto, N. Borisenko, F. Endres, *J. Phys. Chem. C* **2009**, *113*, 13266–13272; c) T. Carstens, R. Hayes, S. Z. El Abedin, B. Corr, G. B. Webber, N. Borisenko, R. Atkin, F. Endres, *Electrochim. Acta* **2012**, *82*, 48–59; d) R. Hayes, N. Borisenko, M. K. Tam, P. C. Howlett, F. Endres, R. Atkin, *J. Phys. Chem. C* **2011**, *115*, 6855–6863; e) K. C. Jha, H. Liu, M. R. Bockstaller, H. Heinz, *J. Phys. Chem. C* **2013**, *117*, 25969–25981; f) Y.-X. Zhong,

 © 2015 Wiley-VCH Verlag GmbH & Co. KGaA, Weinheim

J.-W. Yan, M.-G. Li, X. Zhang, D.-W. He, B.-W. Mao, *J. Am. Chem. Soc.* **2014**, *136*, 14682 – 14685.
[5] a) M. V. Fedorov, R. M. Lynden-Bell, *Phys. Chem. Chem. Phys.* **2012**, *14*, 2552 – 2556; b) R. M. Lynden-Bell, A. I. Frolov, M. V. Fedorov, *Phys. Chem. Chem. Phys.* **2012**, *14*, 2693 – 2701; c) C. Merlet, B. Rotenberg, P. A. Madden, M. Salanne, *Phys. Chem. Chem. Phys.* **2013**, *15*, 15781 – 15792.
[6] a) X. Zhang, Y.-X. Zhong, J.-W. Yan, Y.-Z. Su, M. Zhang, B.-W. Mao, *Chem. Commun.* **2012**, *48*, 582 – 584; b) T. Carstens, R. Gustus, O. Hoefft, N. Borisenko, F. Endres, H. Li, R. J. Wood, A. J. Page, R. Atkin, *J. Phys. Chem. C* **2014**, *118*, 10833 – 10843.
[7] a) F. Buchner, K. Forster-Tonigold, B. Uhl, D. Alwast, N. Wagner, H. Farkhondeh, A. Gross, R. J. Behm, *Acs Nano* **2013**, *7*, 7773 – 7784; b) B. Uhl, F. Buchner, D. Alwast, N. Wagner, R. J. Behm, *Beilstein J. Nanotechnol.* **2013**, *4*, 903 – 918; c) B. Uhl, F. Buchner, S. Gabler, M. Bozorgchenani, R. J. Behm, *Chem. Commun.* **2014**, *50*, 8601 – 8604; d) T. Waldmann, H.-H. Huang, H. E. Hoster, O. Hoefft, F. Endres, R. J. Behm, *ChemPhysChem* **2011**, *12*, 2565 – 2567.
[8] V. O. Santos, Jr., M. B. Alves, M. S. Carvalho, P. A. Z. Suarez, J. C. Rubim, *J. Phys. Chem. B* **2006**, *110*, 20379 – 20385.
[9] a) A. J. Carmichael, C. Hardacre, J. D. Holbrey, M. Nieuwenhuyzen, K. R. Seddon, *Mol. Phys.* **2001**, *99*, 795 – 800; b) E. Sloutskin, E. Solutskin, B. M. Ocko, L. Tamam, L. Taman, I. Kuzmenko, T. Gog, M. Deutsch, *J. Am. Chem. Soc.* **2005**, *127*, 7796 – 7804; c) Y. Lauw, M. D. Horne, T. Rodopoulos, V. Lockett, B. Akgun, W. A. Hamilton, A. R. J. Nelson, *Langmuir* **2012**, *28*, 7374 – 7381.
[10] a) Y.-Z. Su, Y.-C. Fu, J.-W. Yan, Z.-B. Chen, B.-W. Mao, *Angew. Chem. Int. Ed.* **2009**, *48*, 5148 – 5151; *Angew. Chem.* **2009**, *121*, 5250 – 5253; b) G.-B. Pan, W. Freyland, *Chem. Phys. Lett.* **2006**, *427*, 96 – 100; c) M. Gnahm, C. Berger, M. Arkhipova, H. Kunkel, T. Pajkossy, G. Maas, D. M. Kolb, *Phys. Chem. Chem. Phys.* **2012**, *14*, 10647 – 10652; d) M. Gnahm, C. Mueller, R. Repanszki, T. Pajkossy, D. M. Kolb, *Phys. Chem. Chem. Phys.* **2011**, *13*, 11627 – 11633; e) M. Gnahm, T. Pajkossy, D. M. Kolb, *Electrochim. Acta* **2010**, *55*, 6212 – 6217.
[11] a) O. M. Magnussen, W. Polewska, L. Zitzler, R. J. Behm, *Faraday Discuss.* **2002**, *121*, 43 – 52; b) O. M. Magnussen, L. Zitzler, B. Gleich, M. R. Vogt, R. J. Behm, *Electrochim. Acta* **2001**, *46*, 3725 – 3733; c) T. Tansel, O. M. Magnussen, *Phys. Rev. Lett.* **2006**, *96*, 026101; d) A. Taranovskyy, T. Tansel, O. M. Magnussen, *Phys. Rev. Lett.* **2010**, *104*, 106101; e) Y.-C. Yang, A. Taranovskyy, O. M. Magnussen, *Angew. Chem. Int. Ed.* **2012**, *51*, 1966 – 1969; *Angew. Chem.* **2012**, *124*, 2003 – 2007.
[12] D. R. MacFarlane, P. Meakin, J. Sun, N. Amini, M. Forsyth, *J. Phys. Chem. B* **1999**, *103*, 4164 – 4170.
[13] B. Uhl, T. Cremer, M. Roos, F. Maier, H.-P. Steinrueck, J. Behm, *Phys. Chem. Chem. Phys.* **2013**, *15*, 17295 – 17302.
[14] S. Rivera-Rubero, S. Baldelli, *J. Phys. Chem. B* **2004**, *108*, 15133 – 15140.
[15] X. Paredes, J. Fernandez, A. A. H. Padua, P. Malfreyt, F. Malberg, B. Kirchner, A. S. Pensado, *J. Phys. Chem. B* **2014**, *118*, 731 – 742.
[16] a) X. P. Gao, G. J. Edens, M. J. Weaver, *J. Phys. Chem.* **1994**, *98*, 8074 – 8085; b) J. X. Wang, G. M. Watson, B. M. Ocko, *J. Phys. Chem.* **1996**, *100*, 6672 – 6677.
[17] A. A. Kornyshev, *J. Phys. Chem. B* **2007**, *111*, 5545 – 5557.

Received: April 10, 2015
Published online: April 27, 2015

 © 2015 Wiley-VCH Verlag GmbH & Co. KGaA, Weinheim